

ParalESN: Enabling parallel information processing in Reservoir Computing

Matteo Pinna ^{*1} Giacomo Lagomarsini ^{*1} Andrea Ceni ¹ Claudio Gallicchio ¹

Abstract

Reservoir Computing (RC) has established itself as an efficient paradigm for temporal processing. However, its scalability remains severely constrained by (i) the necessity of processing temporal data sequentially and (ii) the prohibitive memory footprint of high-dimensional reservoirs. In this work, we revisit RC through the lens of structured operators and state space modeling to address these limitations, introducing Parallel Echo State Network (ParalESN). ParalESN enables the construction of high-dimensional and efficient reservoirs based on diagonal linear recurrence in the complex space, enabling parallel processing of temporal data. We provide a theoretical analysis demonstrating that ParalESN preserves the Echo State Property and the universality guarantees of traditional Echo State Networks while admitting an equivalent representation of arbitrary linear reservoirs in the complex diagonal form. Empirically, ParalESN matches the predictive accuracy of traditional RC on time series benchmarks, while delivering substantial computational savings. On 1-D pixel-level classification tasks, ParalESN achieves competitive accuracy with fully trainable neural networks while reducing computational costs and energy consumption by orders of magnitude. Overall, ParalESN offers a promising, scalable, and principled pathway for integrating RC within the deep learning landscape.

1. Introduction

Reservoir Computing (RC) has emerged as a simple yet powerful paradigm for harnessing the rich dynamics of recurrent systems for learning and prediction (Nakajima & Fischer, 2021; Lukoševičius & Jaeger, 2009). By fixing

^{*}Equal contribution. ¹Department of Computer Science, University of Pisa, Italy. Correspondence to: Matteo Pinna <matteo.pinna@di.unipi.it>, Giacomo Lagomarsini <giacomo.lagomarsini@phd.unipi.it>.

Preprint. February 2, 2026.

a non-linear recurrent reservoir and training only a linear readout, RC offers favorable training efficiency, strong performance on temporal processing tasks, and intriguing connections to both neuroscience and dynamical systems theory. These properties have led to its success in a wide range of domains, from speech recognition to chaotic signal prediction. Despite these strengths, RC faces the same problem of traditional, fully-trainable Recurrent Neural Networks (RNNs): the input signal has to be processed sequentially, which makes training slow and not parallelizable. In an attempt to improve the efficiency of RC, structured operators have been investigated (Rodan & Tino, 2011; Dong et al., 2020; D’Inverno & Dong, 2025). A particularly active research area involves exploring RC implementations in hardware implementations (Gallicchio & Soriano, 2025). An important theoretical insight is that even *linear* reservoirs, provided that the readout is expressive enough, are universal approximators in the class of fading memory filters (Grigoryeva & Ortega, 2018a;b), thus being able to represent well arbitrary input-output dynamics.

In this work, we address limitations of classical RC by introducing Parallel Echo State Networks (ParalESN), a novel class of efficient untrained RNNs with diagonal linear recurrence in the complex space, where the recurrence can be parallelized via associative scan. Fig. 1 graphically highlights the proposed model. Our approach rethinks reservoir construction through the lens of structured operators. By combining the dynamical richness of RC with the linear recurrence from Linear Recurrent Unit (LRU) (Orvieto et al., 2023), we bridge a gap between classical dynamical systems-inspired learning and contemporary large-scale modeling.

The remainder of this work is organized as follows. Section 2 discusses related works. Section 3 presents the proposed approach, ParalESN. Section 4 presents our theoretical analysis. Section 5 presents the experiments. Finally, Section 6 concludes the paper. In the Appendix, we provide mathematical proofs, definitions, and additional experiments. See Appendix A for a table of contents.

2. Related works

Reservoir Computing. Reservoir Computing (RC) (Verstraeten et al., 2007; Nakajima & Fischer, 2021) is a pop-

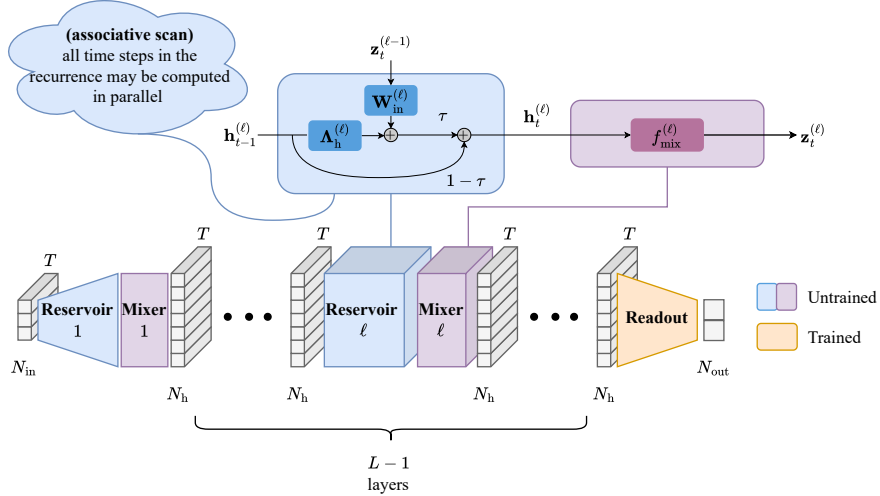


Figure 1. Architectural organization of the proposed ParalESN. The model may have multiple blocks consisting of two components: (i) a linear reservoir and (ii) a non-linear mixing layer. The first block processes the external input as in a traditional shallow architecture. Subsequent blocks process the output of the previous block’s mixing layer, $z_t^{(\ell-1)}$. The structure of the reservoir (in blue) includes a diagonal, complex-valued transition matrix $\Lambda_h^{(\ell)}$ and a dense complex-valued input weight matrix $W_{in}^{(\ell)}$. The main branch and the temporal residual connections are scaled by a positive coefficient τ and $1 - \tau$, respectively. The mixing layer (in purple) is used to introduce non-linearity in the model’s dynamics and to mix the components of the reservoir states at each time step. The readout (in orange) is the only trainable component in the system. See Section 3 for details.

ular framework for the design of efficient untrained Recurrent Neural Networks (RNNs), developed to address the instabilities of training RNNs (Bengio et al., 1994; Glorot & Bengio, 2010; Pascanu et al., 2013). An RC model consists of two main components: (i) a high-dimensional recurrent layer, called *reservoir*, that is randomly initialized and then left untrained, and (ii) a trainable readout layer, that may be trained via lightweight closed-form solutions. Therefore, by design, RC models bypass backpropagation and related vanishing/exploding gradients, and can be trained exceptionally fast in a single forward pass.

Echo State Networks (ESNs) (Jaeger et al., 2007) established themselves as one of the most successful instance of RC models. ESNs dynamics can be defined as follows:

$$\mathbf{h}_t = (1 - \tau)\mathbf{h}_{t-1} + \tau \sigma(\mathbf{W}_h \mathbf{h}_{t-1} + \mathbf{W}_{in} \mathbf{x}_t + \mathbf{b}). \quad (1)$$

where $\mathbf{h}_t \in \mathbb{R}^{N_h}$ and $\mathbf{x}_t \in \mathbb{R}^{N_{in}}$ are, respectively, the state and the external input at time step t . The transition matrix is denoted as $\mathbf{W}_h \in \mathbb{R}^{N_h \times N_h}$, the input weight matrix is denoted as $\mathbf{W}_{in} \in \mathbb{R}^{N_h \times N_{in}}$, $\mathbf{b} \in \mathbb{R}^{N_h}$ denotes the bias vector, σ denotes an element-wise applied non-linearity, and $\tau \in (0, 1]$ denotes the leaky rate hyperparameter. The entries of the matrix \mathbf{W}_{in} and \mathbf{b} are generally sampled randomly from a uniform distribution (Gallicchio et al., 2017; Ceni & Gallicchio, 2024) over $[-\omega_{in}, \omega_{in}]$ and $[-\omega_b, \omega_b]$, respectively. Sampling their entries from Gaussian distri-

butions is also popular (Verstraeten et al., 2007). The entries of \mathbf{W}_h are randomly sampled from a uniform distribution over $[-1, 1]$ and then rescaled to have a desired spectral radius ρ^1 . In practical applications, the spectral radius is generally constrained to be smaller than 1.

The final output is retrieved through the linear readout:

$$\mathbf{y}_t = \mathbf{W}_{out} \mathbf{h}_t + \mathbf{b}_{out}. \quad (2)$$

where $\mathbf{y}_t \in \mathbb{R}^{N_{out}}$ denotes the network output at time step t , and $\mathbf{W}_{out} \in \mathbb{R}^{N_{out} \times N_h}$ and $\mathbf{b}_{out} \in \mathbb{R}^{N_{out}}$ denote the readout weight matrix and bias vector, respectively. The readout is typically optimized via lightweight closed-form solutions, e.g. ridge regression or least squares methods.

The model’s state update function defined in (1) could depend, in principle, from the initial point \mathbf{h}_0 . This leads to non-deterministic behaviors, i.e. the impossibility to determine the state solely from the inputs. To avoid that, the reservoir in ESNs is initialized subject to the Echo State Property (ESP) (Yildiz et al., 2012), a useful stability condition for guiding ESN initialization. We say that a discrete time dynamical system defined by the transition function $F(\mathbf{h}, \mathbf{x})$ satisfies the ESP if the states asymptotically depends only on the system’s inputs. In other words, for any

¹The spectral radius of a matrix \mathbf{A} , denoted $\rho(\mathbf{A})$, is defined as the largest among the lengths of its eigenvalues.

two initial points \mathbf{h}_0 and \mathbf{h}'_0 , then

$$\lim_{t \rightarrow \infty} \|F(\mathbf{h}_{t-1}, \mathbf{x}_t) - F(\mathbf{h}'_{t-1}, \mathbf{x}_t)\|_2 = 0. \quad (3)$$

Several ESN variants lay their foundation at the intersection of the RC and DL frameworks. In particular, Deep Echo State Networks (DeepESNs) (Gallicchio et al., 2017) generalize the concept of shallow ESNs towards deep architectural constructions, where multiple untrained reservoirs are stacked on top of each other. The increased feed-forward depth has been shown to provide advantageous architectural bias relative to shallow ESNs. More recently, Residual Echo State Networks (ResESNs) (Ceni & Gallicchio, 2024) introduced orthogonal residual connections along the temporal dimension to enhance long-term information processing capabilities. Other works have explored structured transforms to improve the efficiency of RC, including Simple Cycle Reservoir (SCR) (Rodan & Tino, 2011), where the transition matrix employs a fixed ring topology, and Structured Reservoir Computing (Structured RC) (Dong et al., 2020), where the transition matrix consists of a composition of Hadamard and diagonal matrices.

Universality of linear reservoirs. ESP guarantees the universality of the reservoir system in approximating fading memory filters (Grigoryeva & Ortega, 2018a). Provided that the ESP holds, similar universality results have also been proven for reservoirs characterized by linear dynamics, when combined with non-linear readouts that universally approximate functions $f : \mathbb{C}^{N_h} \rightarrow \mathbb{C}^{N_y}$ (Grigoryeva & Ortega, 2018b; Gonon & Ortega, 2020). Therefore, linear recurrence ESNs, in combination with non-linear readouts, can approximately arbitrarily well any time-invariant causal filter with the fading memory property.

Transformers. Transformers are the de-facto standard architecture for sequence modeling, managing to replace recurrent models on real-world tasks since their introduction in (Vaswani et al., 2017). Differently from RNNs, transformers are a feedforward architecture, and employ self-attention, enabling access to every position of the sequence at any time. This allows for great parallelization and modeling capacity, but comes at a cost of a quadratic complexity in sequence length, making scaling to long contexts challenging. To address this issue, many variants to the naive self-attention aiming to lower the computational and memory burden while maintaining expressivity have been proposed (Tay et al., 2022).

State Space Models. Besides training instabilities, another major drawback of stateful sequence models like RNNs is that the input needs to be processed sequentially, greatly limiting the parallelization capabilities of these type of architectures on modern accelerators. One of the most promising approaches for the parallelization of recurrent models is that of (Deep) State Space Models (SSMs) (Gu

et al., 2021). SSMs start from the idea of a linear state space dynamical system, and devise initialization and discretization strategies that help improve memory capacity of the system. Linear recurrence is easily parallelizable (see e.g. Martin & Cundy, 2018), greatly improving training and inference efficiency of this family of models. Structured SSMs such as S4 and S5 (Gu et al., 2021; Smith et al., 2022) demonstrated how linear recurrence, along with a careful initialization based on HiPPO matrices (Gu et al., 2020), can enhance long memory propagation on long sequence tasks. Building on these foundations, Mamba (Gu & Dao, 2024; Dao & Gu, 2024) proposes a selective architecture that allows to change the dynamic based on its inputs. These advances position SSMs as contenders to transformers in sequence modeling, particularly in tasks demanding long memory retention.

Linear recurrent unit. Linear recurrent Unit (LRU) (Orvieto et al., 2023) successfully applied linear recurrence to general RNNs, demonstrating that it is possible to deviate from the strict initialization and parametrization rules of SSMs, while retaining their impressive performance. Rather than initializing matrices using HiPPO theory as standard SSMs, LRU employs a diagonal transition matrix, whose eigenvalues are initialized inside the unitary complex disk, using a de-coupled parametrization of their magnitude and phase. In particular, the magnitude is chosen in an interval $[r_{\min}, r_{\max}]$, which allows a finer control over stability and memory capacity of the model. The linear, diagonal structure reduces recurrent updates to parallelizable element-wise operations, and the initialization strategy makes the architecture more stable for longer sequences.

3. ParalESN

Inspired by the success of SSMs, we design a more scalable and efficient reservoir architecture, which we call *ParalESN*. ParalESN improves upon previous RC models by employing a linear diagonal recurrence, similar to that of LRU, followed by a mixing function that combines reservoir states. As is standard in the RC paradigm, only the readout function is trainable. We also explore a *deep* variant of ParalESN, which we denote ParalESN (deep). See Fig. 1 for a graphical representation of the architecture.

Let $\mathbf{z}_t^{(0)} = \mathbf{x}_t$ denote the input to the first layer. The reservoir dynamics at layer ℓ are described by:

$$\mathbf{h}_t^{(\ell)} = (1 - \tau^{(\ell)}) \mathbf{h}_{t-1}^{(\ell)} + \tau^{(\ell)} \left(\mathbf{A}_h^{(\ell)} \mathbf{h}_{t-1}^{(\ell)} + \mathbf{W}_{\text{in}}^{(\ell)} \mathbf{z}_t^{(\ell-1)} + \mathbf{b}^{(\ell)} \right), \quad (4)$$

where superscript (ℓ) denotes layer-specific hyperparameters and weights. For each time step $t \in \{1, \dots, T\}$, $\mathbf{x}_t \in \mathbb{R}^{N_{\text{in}}}$ is the external input, $\mathbf{h}_t^{(\ell)} \in \mathbb{C}^{N_h}$ is the reservoir state, and $\mathbf{z}_t^{(\ell)} \in \mathbb{R}^{N_h}$ is the hidden state after the mixing

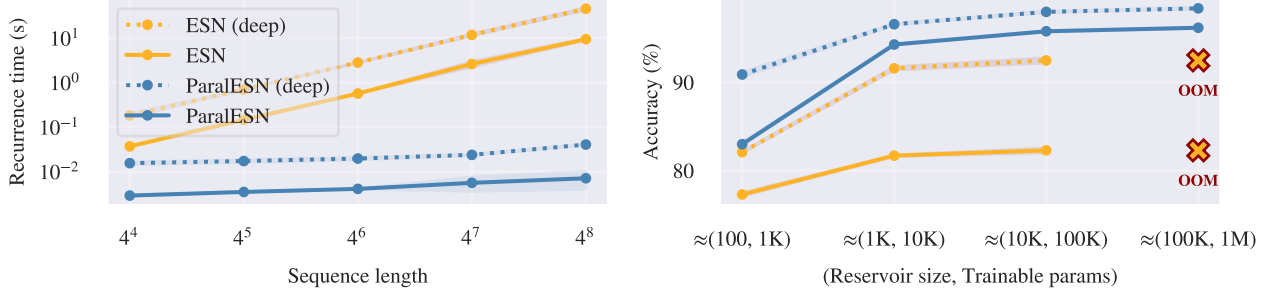


Figure 2. (left) Time required to perform the recurrence in ParalESN and traditional ESNs for increasing sequence lengths, assuming 128 recurrent neurons and 5 layers for deep configurations. ParalESN scales logarithmically with sequence length, whereas traditional ESNs scale linearly. (right) Scaling ParalESN and traditional ESNs to high-dimensional reservoirs on the sMNIST task. Traditional ESNs run out-of-memory (OOM) at approximately 100K reservoir neurons, while ParalESN fit into memory due to the reduced memory footprint of their diagonal transition matrices.

step. The matrix $\Lambda_h^{(\ell)} \in \mathbb{C}^{N_h \times N_h}$ is a diagonal transition matrix, $\mathbf{b}^{(\ell)} \in \mathbb{C}^{N_h}$ is the bias vector, and $\tau^{(\ell)} \in (0, 1]$ is the leaky rate. Since the recurrence is linear, the leaky integration can be partially absorbed into the transition matrix. Accounting for leakage, the effective transition matrix becomes $\Lambda^{(\ell)}_h = (1 - \tau^{(\ell)})\mathbf{I} + \tau^{(\ell)}\Lambda_h^{(\ell)}$, where \mathbf{I} is the identity matrix. The input weight matrix $\mathbf{W}_{\text{in}}^{(1)} \in \mathbb{C}^{N_h \times N_{\text{in}}}$ is dense for the first layer, mapping the external input to the hidden dimension. For subsequent layers, the input weight matrix $\mathbf{W}_{\text{in}}^{(\ell>1)} \in \mathbb{C}^{N_h \times N_h}$ employs the following ring topology (Rodan & Tino, 2011; Verzelli et al., 2020; Tino, 2020; Pinna et al., 2025) to reduce memory overhead:

$$\mathbf{W}_{\text{in}}^{(\ell>1)} = \begin{bmatrix} 0 & 0 & \cdots & 0 & w_1 \\ w_2 & 0 & \cdots & 0 & 0 \\ 0 & w_3 & \cdots & 0 & 0 \\ \vdots & \vdots & \ddots & \vdots & \vdots \\ 0 & 0 & \cdots & w_{N_h} & 0 \end{bmatrix}, \quad (5)$$

The matrix in (5) shifts the input vector and then applies an element-wise scaling. Consequently, we only store a N_h -dimensional vector of scaling coefficients, significantly reducing the memory footprint in deeper layers. The entries of the input weight matrices are initialized by sampling the real and imaginary parts independently from a uniform distribution over $[-1, 1]$ and then scaling each row i of the matrix by $\sqrt{1 - |\lambda_i|^2}$, where λ_i is the corresponding diagonal element (eigenvalue) of the transition matrix $\Lambda_h^{(\ell)}$. The bias vectors are sampled from a uniform distribution and scaled by hyperparameter $\omega_b^{(\ell)}$. The diagonal elements of the transition matrix are initialized to control the eigenvalue distribution, with spectral radii sampled uniformly from $[\rho_{\min}^{(\ell)}, \rho_{\max}^{(\ell)}]$ and phases from $[\theta_{\min}^{(\ell)}, \theta_{\max}^{(\ell)}]$, forming complex eigenvalues $\rho^{(\ell)} e^{i\theta^{(\ell)}}$.

The mixing function f_{mix} introduces non-linearity into the model and enables interaction among the components of

the hidden state, which would otherwise evolve independently due to the diagonal structure of the recurrence. The mixing function is defined as:

$$\mathbf{z}_t^{(\ell)} = f_{\text{mix}}(\mathbf{h}_t^{(\ell)}) = \tanh \left(\Re \left(\mathbf{W}_{\text{mix}}^{(\ell)} * \mathbf{h}_t^{(\ell)} + \mathbf{b}_{\text{mix}}^{(\ell)} \right) \right), \quad (6)$$

where $*$ denotes the convolution operator, $\mathbf{W}_{\text{mix}}^{(\ell)} \in \mathbb{C}^k$ is a 1-D kernel of size $k^{(\ell)}$, $\mathbf{b}_{\text{mix}}^{(\ell)} \in \mathbb{C}$ is a scalar bias, and $\Re(\cdot)$ extracts the real part. The kernel slides across the hidden dimension of $\mathbf{h}_t^{(\ell)} \in \mathbb{C}^{N_h}$ with same-padding, producing an output of identical dimension. We employ a 1-D convolution rather than a dense matrix, to reduce the memory footprint of the mixing function. The same kernel is shared across all time steps, requiring only $k + 1$ parameters regardless of sequence length or hidden size. The kernel and bias entries are sampled randomly from a uniform distribution over $[-\omega_{\text{mix}}^{(\ell)}, \omega_{\text{mix}}^{(\ell)}]$ and $[-\omega_{\text{mixb}}^{(\ell)}, \omega_{\text{mixb}}^{(\ell)}]$, respectively.

The readout layer aggregates the mixed states from all L layers:

$$\mathbf{y}_t = f_{\text{readout}}(\mathbf{z}_t^{(1)}, \dots, \mathbf{z}_t^{(L)}) \quad (7)$$

For classification tasks, only the final time step is used, $\mathbf{y} = f_{\text{readout}}(\mathbf{z}_T^{(1)}, \dots, \mathbf{z}_T^{(L)})$.

Fig. 2 graphically demonstrates ParalESN's speed advantage over traditional ESNs with respect to sequence length (left) and its ability to scale to high-dimensional reservoirs (right). ParalESN's recurrence time scales logarithmically with sequence length, rather than linearly, due to its ability to parallelize the recurrence. Note that even the deep configuration of ParalESN is consistently faster than the shallow configuration of ESN, despite consisting of a higher number of reservoir layers. Additionally, by employing a diagonal transition matrix, ParalESN can scale to higher-dimensional reservoirs compared to traditional RC, which generally employs dense $N_h \times N_h$ transition matrices. See Appendix B for a computational complexity analysis of

ParalESN and other RC approaches. ParalESN achieves lower time complexity, reducing it from linear to logarithmic with respect to sequence length, and the memory footprint of its parameters doesn't scale quadratically with respect to the hidden size (see Table 5).

4. Theoretical Analysis

In this section, we derive a simple condition for the ESP to hold. The ESP is necessary to prove a result of universality for the class of linear reservoir models (Grigoryeva & Ortega, 2018a).

We consider a one-layer ParalESN. The sequence of hidden states produced by the model given a sequence of inputs $\{\mathbf{x}_1, \dots, \mathbf{x}_T\} \in (\mathbb{C}^{N_{\text{in}}})^T$ and a starting point $\mathbf{h}_0 \in \mathbb{C}^{N_{\text{h}}}$ is $(\mathbf{y}_0, \dots, \mathbf{y}_T)$, with

$$\mathbf{h}_t = \begin{cases} \mathbf{h}_0 & \text{if } t = 0 \\ \bar{\Lambda}_h \mathbf{h}_{t-1} + \tau(\mathbf{W}_{\text{in}} \mathbf{x}_t + \mathbf{b}) & \text{oth.} \end{cases} \quad (8)$$

$$\mathbf{y}_t = f_{\text{out}}(\mathbf{h}_t), \quad (9)$$

where f_{out} is the readout function. Because the recurrence is linear, the readout function must be non-linear to preserve expressivity. This definition apparently differs slightly from equations (4), (6), and (7), but since training does not come into play in this section, we can incorporate f_{mix} and f_{readout} in a single function f_{out} .

4.1. Echo State Property

As a first step of the theoretical analysis, we show that it is easy to derive a simple condition for the ESP to hold in the case of linear ESN of (8). The same condition on the spectral radius that is necessary for the ESP of ESNs (see, e.g., (Jaeger & Haas, 2004)) is also sufficient in our case. Moreover, in the case of a diagonal transition matrix, we can directly control the spectral radius by examining the largest diagonal value in modulus.

Theorem 4.1 (Sufficient and necessary conditions for the ESP). *A ParalESN has the ESP if and only if the diagonal elements $\lambda_1, \dots, \lambda_{N_h}$ of the transition matrix $\bar{\Lambda}_h$ are such that for each i , $|\lambda_i| < 1$, where $|\cdot|$ is the complex modulus.*

The proof is given in Appendix C.1.

4.2. Expressivity of ParalESN

An ESN with linear recurrence and MLP readout and the ESP property is universal in the family of fading memory filters, and in particular it is as powerful as non-linear ESNs, that have the same property (Grigoryeva & Ortega, 2018a;b) (see also Appendix D for definitions on fading memory filters). We have stated the conditions for ParalESN to have the ESP property in Theorem 4.1. We

now show that an ParalESN is as expressive as a ESN with linear recurrence and any arbitrary transition matrix $\mathbf{W}_h \in \mathbb{C}^{N_h \times N_h}$ and MLP readout.

Proposition 4.2. *Consider an ESN with linear recurrence and a 1-layer MLP readout, defined by*

$$\begin{cases} \mathbf{h}_t = \mathbf{W}_h \mathbf{h}_{t-1} + \mathbf{W}_{\text{in}} \mathbf{x}_t \\ \mathbf{y}_t = \mathbf{W}_{\text{out}}(\sigma(\mathbf{W}_h \mathbf{h}_t)) = \text{MLP}(\mathbf{h}_t) \end{cases} \quad (10)$$

where \mathbf{W}_h , \mathbf{W}_{in} are matrices of appropriate sizes. Then, there exists a ParalESN with MLP readout, defined by (8) and (9) with f_{out} being another MLP, such that for any given input, the two models produce the same output.

The proposition can be proven by diagonalizing the full matrix \mathbf{W}_h . The proof is given in Appendix C.2.

By Proposition 4.2 and results on equivalent expressiveness between ESNs with linear recurrence and standard ESNs, we can deduce that ParalESN and standard ESNs (both with the ESP) are *equivalently expressive*. We explicitly state this fact in the following corollary.

Corollary 4.3. *The class of ParalESN models with the ESP, endowed with an MLP readout, is universal in the family of fading memory filters.*

In practice, in our experiments, the MLP readout is often decomposed into two layers: the first layer, together with the non-linearity, is treated as the fixed mixing function, the last layer is treated as the trainable readout.

5. Experiments

We empirically validate the performance of the proposed approach on time series regression and classification tasks (see also Appendix E), and with respect to traditional RC and fully-trainable sequence models. As our fully-trainable models, we consider a LSTM, a standard Transformer (Vaswani et al., 2017), a Linear Recurrent Unit (LRU) (Orvieto et al., 2023)², and Mamba (Gu & Dao, 2024)³ to cover a wide range of model classes, including recurrent neural networks, attention-based neural networks, and deep state space models, respectively. See Appendix F for details on the experimental setting and Appendix G for experiments on hyperparameters' sensitivity and comparison with other structured RC approaches.

Comparison with respect to traditional RC. Fig. 3 compares ParalESN provides with respect to traditional RC from performance and efficiency perspectives. The left panels presents the trade-off between performance and efficiency, the right panel presents a critical difference plot ranking models based on their overall performance. We

²Code from github.com/NicolasZucchet/minimal-LRU.

³Code from github.com/state-spaces/mamba.

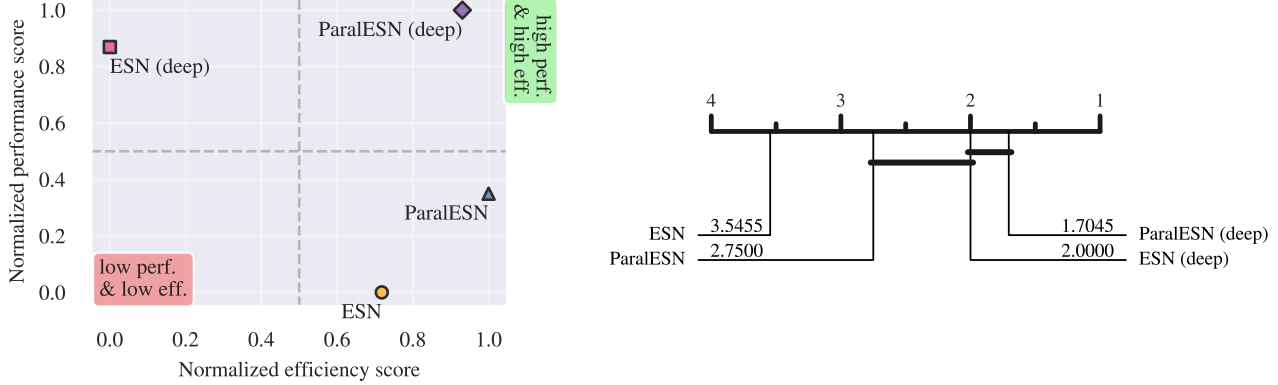


Figure 3. (left) Analysis of the trade-off between performance (error for regression tasks and accuracy for classification tasks) and efficiency (training time) for ParalESN and traditional ESNs across all considered benchmarks. For each model, we compute the percentage improvement over the ESN baseline for each task. The normalized scores are then obtained via min-max normalization of these average improvements, mapping them to a $[0, 1]$ scale, where 0 corresponds to the worst-performing model and 1 to the best-performing one. Overall, ParalESN and ParalESN (deep) outperform their counterparts while being more efficient. (right) Critical difference plot computed via a Wilcoxon test (Demšar, 2006), showing the average rank (lower is better). Models are ranked based on their overall performance across all benchmarks. Cliques (solid lines) connect models for which there is no statistically significant difference in performance. On average, ParalESN (deep) is the top-performing model.

observe that ParalESN is both more accurate and more efficient with respect to its counterpart (shallow or deep). In particular, ParalESN (deep), despite consisting of multiple reservoir layers, is able to stay competitive in terms of recurrence speed with respect to a shallow ESN. Additionally, ParalESN outperforms its shallow counterpart by a statistically significant margin. Although there is not statistically significant difference between the performance of ParalESN (deep) and ESN (deep), the former is the top-performing model while being considerably more efficient.

5.1. Time series regression

Memory-based tasks are designed to assess the model’s ability to recall delayed versions of the input, while forecasting tasks evaluate the model’s ability to predict future time steps. We consider MemCap (Jaeger, 2001), ctXOR (Verstraeten et al., 2010), and SinMem (Inubushi & Yoshimura, 2017) in our memory-based benchmark. For our forecasting benchmark, we consider Lorenz96 (Lorenz, 1996), Mackey-Glass (MG) (Jaeger & Haas, 2004), NARMA, and a selection of real-world time series forecasting tasks from (Zhou et al., 2021), including ETTh1, ETTh2, ETTm1, and ETTm2.

Discussion. Table 1 and Table 2 present the test set results on memory-based and forecasting tasks, respectively. Fig. 4 graphically compares the training time of ParalESN to that to traditional ESNs. Our experiments demonstrate that ParalESN can achieve comparable results to traditional RC across a wide range of time series regression benchmarks, while offering exceptional advantages from a com-

putational efficiency perspective. In all benchmarks, ParalESN trains an entire order of magnitude faster, except for Lorenz25 and Lorenz50, where the relatively small sequence length reduces the advantage of being able to parallelize the recurrence. Observe that even ParalESN (deep), despite consisting of multiple reservoir layers, trains faster than a traditional, shallow ESN consisting of just one layer. Indeed, while the readout layer is trained via Ridge regression in both cases, the time required to perform the recurrence through the untrained reservoir is significantly lower in the proposed approach compared to traditional ESNs, thanks to being able to process the sequence in parallel.

5.2. Time series classification

The time series classification benchmark consists of a selection of tasks from the UEA & UCR repository (Bagnall et al., 2018; Dau et al., 2019). For 1-D pixel-level classification, we consider two variations of the MNIST dataset (LeCun, 1998): (i) sequential MNIST (sMNIST), where pixels are flattened into a one-dimensional vector, and (ii) permuted sequential MNIST (psMNIST), where on top of the flattening a random permutation is applied to the pixels.

Discussion. Tables 3 and 4 present test set results on time series classification tasks from the UEA & UCR repository and on sMNIST and psMNIST, respectively. Fig. 5 visualizes the trade-off between performance and efficiency among all models for the MNIST benchmarks. On time series classification, ParalESN achieves higher test accuracy compared to a shallow ESN: +27.9% on Blink, +3.7% on FaultDetectionA, +7.6% on FordA, +5.7% on FordB, and

Table 1. Test set results of memory-based tasks, assuming 128 recurrent neurons for each model. The **best result** is highlighted in bold.

MEMORY-BASED	MEMCAP (\uparrow)	$\cdot 10^{-1}$ CTXOR5 (\downarrow)	$\cdot 10^{-1}$ CTXOR10 (\downarrow)	$\cdot 10^{-1}$ SINMEM10 (\downarrow)	$\cdot 10^{-1}$ SINMEM20 (\downarrow)
ESN	50.6 ± 1.6	3.6 ± 0.1	7.7 ± 0.6	3.6 ± 0.1	3.7 ± 0.1
ESN (deep)	56.8 ± 1.3	3.4 ± 0.2	5.2 ± 1.0	1.2 ± 0.1	1.6 ± 0.1
ParalESN	114.5 ± 1.4	3.9 ± 0.1	8.2 ± 0.2	3.7 ± 0.0	3.7 ± 0.0
ParalESN (deep)	125.0 ± 0.2	3.6 ± 0.1	5.6 ± 0.4	1.0 ± 0.2	2.5 ± 0.4

 Table 2. Test set results of forecasting tasks, assuming 128 recurrent neurons for each model. The **best result** is highlighted in bold.

FORECASTING	$\cdot 10^{-2}$ Lz25 (\downarrow)	$\cdot 10^{-2}$ Lz50 (\downarrow)	$\cdot 10^{-4}$ MG (\downarrow)	$\cdot 10^{-2}$ MG84 (\downarrow)	$\cdot 10^{-2}$ N10 (\downarrow)	$\cdot 10^{-2}$ N30 (\downarrow)	$\cdot 10^{-1}$ ETTh1 (\downarrow)	$\cdot 10^{-1}$ ETTh2 (\downarrow)	$\cdot 10^{-1}$ ETTM1 (\downarrow)	$\cdot 10^{-1}$ ETTM2 (\downarrow)
ESN	10.0 ± 0.3	30.8 ± 0.6	3.0 ± 0.0	6.5 ± 0.4	2.7 ± 0.4	10.3 ± 0.1	9.1 ± 0.2	13.0 ± 1.7	6.7 ± 0.1	9.9 ± 7.3
ESN (deep)	9.7 ± 0.2	30.5 ± 0.3	2.0 ± 0.0	4.2 ± 0.2	3.0 ± 0.5	10.1 ± 0.1	8.9 ± 0.1	9.6 ± 0.5	6.6 ± 0.0	6.0 ± 0.6
ParalESN	10.4 ± 0.5	30.2 ± 0.5	2.8 ± 0.2	7.4 ± 0.4	3.7 ± 0.8	10.2 ± 0.1	9.0 ± 0.2	12.8 ± 1.2	6.5 ± 0.1	5.1 ± 0.1
ParalESN (deep)	10.3 ± 0.3	29.4 ± 0.3	2.6 ± 0.4	5.2 ± 0.5	4.5 ± 1.0	10.2 ± 0.2	8.8 ± 0.1	9.7 ± 0.9	6.5 ± 0.0	5.0 ± 0.0

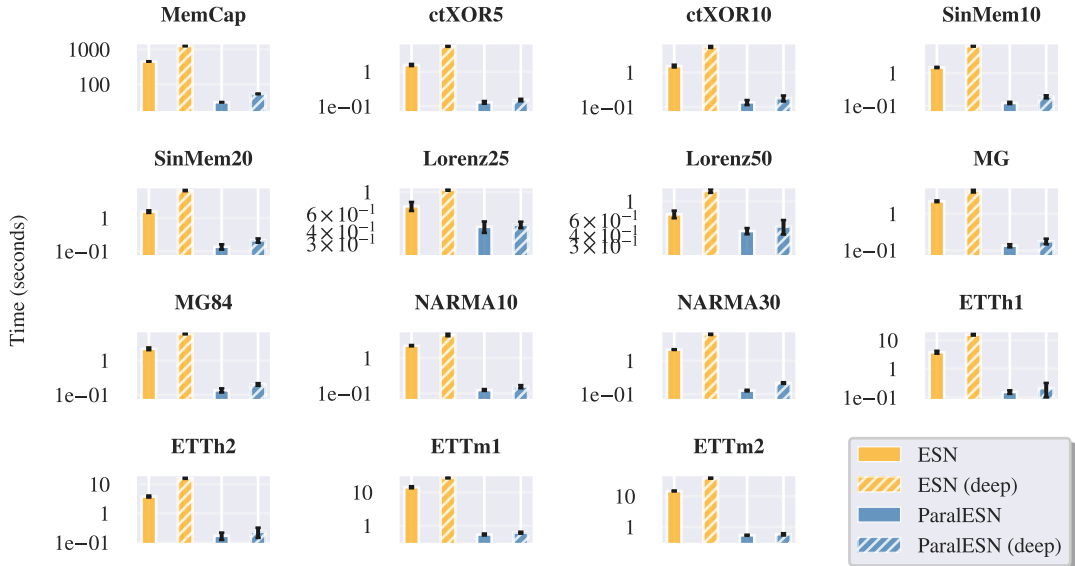


Figure 4. Training time comparison between ParalESNs and traditional ESNs for each memory-based and forecasting benchmark. ParalESN and ParalESN (deep) train order of magnitude faster.

+3.3% on StarLightCurves. Similarly, ParalESN (deep) outperforms ESN (deep) by +10.0% on Blink, +8.8% on FaultDetectionA, +2.7% on FordA, +0.7% on FordB, and +2.3% on StarLightCurves. On sMNIST and psMNIST, ParalESN achieves higher test accuracy by +13.4% and +17.1%, respectively, compared to traditional ESN. ParalESN (deep) provides gains of +7.7% and +13.1% over ESN (deep). These performance improvements come alongside substantial efficiency gains, with ParalESN and ParalESN (deep) requiring half or less of the training time, CO2 emissions, and energy of their counterparts. Unlike traditional RC, ParalESN is competitive with LSTMs, Transformers, LRU, and Mamba, while delivering computational savings of orders of magnitude.

6. Conclusions

We introduced ParalESN, a novel framework for constructing high-dimensional, efficient, and parallelizable untrained RNNs based on linear diagonal recurrence. This work addresses fundamental limitations of traditional RC, including the necessity of processing data sequentially and the prohibitive memory footprint of high-dimensional reservoirs. Results across various time series and 1-D pixel-level classification benchmarks demonstrate that ParalESN is, on average, more accurate and faster than traditional RC, while remaining competitive with fully-trainable sequence models at a fraction of their computational cost.

Table 3. Test set results on time series classification tasks, assuming 1024 recurrent neurons for each model. The **best result** is highlighted in bold.

MODEL	BLINK	FAULTDETECTIONA	FORDA	FORDB	STARLIGHTCURVES
ESN	68.9 ± 5.5	71.3 ± 0.8	75.8 ± 0.9	62.7 ± 0.8	92.1 ± 0.7
ESN (DEEP)	86.5 ± 1.8	86.0 ± 0.6	90.1 ± 0.8	76.1 ± 0.8	93.8 ± 0.4
PARAESN	96.8 ± 1.1	75.0 ± 0.4	83.4 ± 0.7	68.4 ± 1.0	95.4 ± 0.4
PARAESN (DEEP)	96.5 ± 0.4	94.8 ± 0.9	92.8 ± 0.5	76.8 ± 1.6	96.1 ± 0.3

Table 4. Test set results sMNIST and psMNIST tasks. The top-two results are underlined, the **best result** overall is highlighted in bold.

sMNIST					
MODEL	PARAMS.	↑ ACCURACY	↓ TIME (MIN.)	↓ EMISSIONS (KG)	↓ ENERGY (KWH)
LSTM	$\approx 160k$	97.5 ± 1.4	80.8 ± 6.8	0.34 ± 0.14	1.02 ± 0.42
TRANSFORMER	$\approx 160k$	98.4 ± 0.1	141.0 ± 14.1	0.60 ± 0.28	1.81 ± 0.86
LRU	$\approx 160k$	98.5 ± 0.2	29.1 ± 1.85	0.18 ± 0.02	0.57 ± 0.05
MAMBA	$\approx 200k$	98.4 ± 0.1	22.87 ± 4.48	0.19 ± 0.02	0.57 ± 0.06
ESN	$\approx 160k$	82.5 ± 7	4.3 ± 0.1	0.02 ± 0.00	0.07 ± 0.00
ESN (DEEP)	$\approx 160k$	91.4 ± 1.1	8.8 ± 0.1	0.04 ± 0.00	0.13 ± 0.00
PARAESN	$\approx 160k$	96.2 ± 1.3	2.7 ± 0.7	0.01 ± 0.00	0.04 ± 0.1
PARAESN (DEEP)	$\approx 160k$	97.2 ± 0.2	3.3 ± 0.5	0.02 ± 0.00	0.05 ± 0.00

psMNIST					
MODEL	PARAMS.	↑ ACCURACY	↓ TIME (MIN.)	↓ EMISSIONS (KG)	↓ ENERGY (KWH)
LSTM	$\approx 160k$	92.8 ± 0.5	89.3 ± 4.2	0.47 ± 0.04	1.41 ± 0.11
TRANSFORMER	$\approx 160k$	97.4 ± 0.2	156.8 ± 2.7	0.65 ± 0.24	1.98 ± 0.73
LRU	$\approx 160k$	97.8 ± 0.1	33.8 ± 3.42	0.21 ± 0.03	0.63 ± 0.09
MAMBA	$\approx 200k$	92.6 ± 0.1	43.25 ± 5.02	0.24 ± 0.03	0.73 ± 0.08
ESN	$\approx 160k$	78.2 ± 1.6	4.3 ± 0.1	0.02 ± 0.00	0.06 ± 0.00
ESN (DEEP)	$\approx 160k$	82.1 ± 3.7	7.3 ± 0.1	0.04 ± 0.00	0.11 ± 0.00
PARAESN	$\approx 160k$	96.9 ± 0.1	2.8 ± 0.3	0.01 ± 0.00	0.04 ± 0.00
PARAESN (DEEP)	$\approx 160k$	95.2 ± 0.1	3.1 ± 0.2	0.02 ± 0.00	0.05 ± 0.00

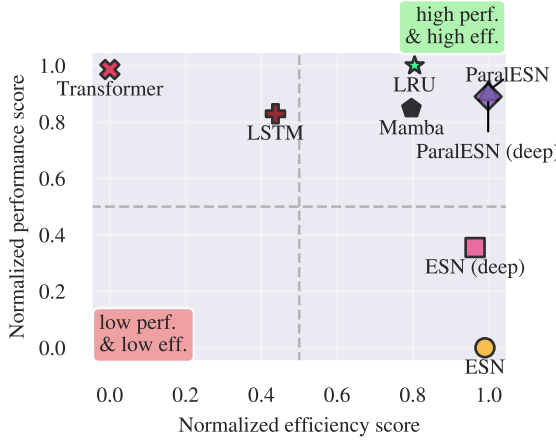


Figure 5. Trade-off between performance (test accuracy) and efficiency (training time) for ParalESN, traditional RC, and fully-trainable sequence models, for the sMNIST and psMNIST benchmarks. For each model and benchmark, we compute the percentage improvement over the ESN baseline. The normalized scores are then obtained via min-max normalization of these average improvements, mapping them to a $[0, 1]$ scale with 0 representing the worst-performing model and 1 the best-performing one. ParalESN is competitive with fully-trainable models while delivering substantial efficiency improvements.

Acknowledgements

This work has been supported by NEURONE, a project funded by the European Union - Next Generation EU, M4C1 CUP I53D23003600006, under program PRIN 2022 (prj. code 20229JRTZA), and by EU-EIC EMERGE (Grant No. 101070918). Computational resources were provided by Computing@Unipi, a computing service of the University of Pisa.

References

Bagnall, A., Dau, H. A., Lines, J., Flynn, M., Large, J., Bostrom, A., Southam, P., and Keogh, E. The uea multivariate time series classification archive, 2018. *arXiv preprint arXiv:1811.00075*, 2018.

Bengio, Y., Simard, P., and Frasconi, P. Learning long-term dependencies with gradient descent is difficult. *IEEE transactions on neural networks*, 5(2):157–166, 1994.

Ceni, A. and Gallicchio, C. Residual echo state networks: Residual recurrent neural networks with stable dynamics and fast learning. *Neurocomputing*, 597:127966, 2024.

Courty, B., Schmidt, V., Goyal-Kamal, MarionCoutarel, Feld, B., Lecourt, J., LiamConnell, SabAmine, inimaz, supatomic, Léval, M., Blanche, L., Cruveiller, A., ouminasara, Zhao, F., Joshi, A., Bogroff, A., Saboni, A., de Lavoreille, H., Laskaris, N., Abati, E., Blank, D., Wang, Z., Catovic, A., alencon, Stechly, M., Bauer, C., Lucas-Otavio, JPW, and MinervaBooks. mlc02/codcarbon: v2.4.1, 2024. URL <https://doi.org/10.5281/zenodo.11171501>.

Dao, T. and Gu, A. Transformers are ssms: generalized models and efficient algorithms through structured state space duality. In *Proceedings of the 41st International Conference on Machine Learning*, ICML’24. JMLR.org, 2024.

Dau, H. A., Bagnall, A., Kamgar, K., Yeh, C.-C. M., Zhu, Y., Gharghabi, S., Ratanamahatana, C. A., and Keogh, E. The ucr time series archive. *IEEE/CAA Journal of Automatica Sinica*, 6(6):1293–1305, 2019.

Demšar, J. Statistical comparisons of classifiers over multiple data sets. *Journal of Machine learning research*, 7 (Jan):1–30, 2006.

Dong, J., Ohana, R., Rafayelyan, M., and Krzakala, F. Reservoir computing meets recurrent kernels and structured transforms. *Advances in Neural Information Processing Systems*, 33:16785–16796, 2020.

D’Inverno, G. A. and Dong, J. Comparison of reservoir computing topologies using the recurrent kernel approach. *Neurocomputing*, 611:128679, 2025.

Gallicchio, C. and Soriano, M. C. Hardware friendly deep reservoir computing. *Neural Networks*, pp. 108079, 2025.

Gallicchio, C., Micheli, A., and Pedrelli, L. Deep reservoir computing: A critical experimental analysis. *Neurocomputing*, 268:87–99, 2017.

Glorot, X. and Bengio, Y. Understanding the difficulty of training deep feedforward neural networks. In *Proceedings of the thirteenth international conference on artificial intelligence and statistics*, pp. 249–256. JMLR Workshop and Conference Proceedings, 2010.

Gonon, L. and Ortega, J.-P. Reservoir computing universality with stochastic inputs. *IEEE Transactions on Neural Networks and Learning Systems*, 31(1):100–112, 2020. doi: 10.1109/TNNLS.2019.2899649.

Grigoryeva, L. and Ortega, J.-P. Echo state networks are universal. *Neural Networks*, 108: 495–508, 2018a. ISSN 0893-6080. doi: <https://doi.org/10.1016/j.neunet.2018.08.025>. URL <https://www.sciencedirect.com/science/article/pii/S089360801830251X>.

Grigoryeva, L. and Ortega, J.-P. Universal discrete-time reservoir computers with stochastic inputs and linear readouts using non-homogeneous state-affine systems. *Journal of Machine Learning Research*, 19:1–40, 09 2018b. doi: 10.48550/arXiv.1712.00754.

Gu, A. and Dao, T. Mamba: Linear-time sequence modeling with selective state spaces. In *First Conference on Language Modeling*, 2024. URL <https://openreview.net/forum?id=tEYskw1VY2>.

Gu, A., Dao, T., Ermon, S., Rudra, A., and Ré, C. Hippo: recurrent memory with optimal polynomial projections. In *Proceedings of the 34th International Conference on Neural Information Processing Systems*, NIPS ’20, Red Hook, NY, USA, 2020. Curran Associates Inc. ISBN 9781713829546.

Gu, A., Goel, K., and Ré, C. Efficiently modeling long sequences with structured state spaces. *arXiv preprint arXiv:2111.00396*, 2021.

Inubushi, M. and Yoshimura, K. Reservoir computing beyond memory-nonlinearity trade-off. *Scientific reports*, 7(1):10199, 2017.

Jaeger, H. Short term memory in echo state networks. 2001.

Jaeger, H. and Haas, H. Harnessing nonlinearity: Predicting chaotic systems and saving energy in wireless communication. *science*, 304(5667):78–80, 2004.

Jaeger, H., Lukoševičius, M., Popovici, D., and Siewert, U. Optimization and applications of echo state networks with leaky-integrator neurons. *Neural networks*, 20(3):335–352, 2007.

LeCun, Y. The mnist database of handwritten digits. <http://yann.lecun.com/exdb/mnist/>, 1998.

Lorenz, E. N. Predictability: A problem partly solved. In *Proc. Seminar on predictability*, volume 1, pp. 1–18. Reading, 1996.

Lukoševičius, M. and Jaeger, H. Reservoir computing approaches to recurrent neural network training. *Computer science review*, 3(3):127–149, 2009.

Martin, E. and Cundy, C. Parallelizing linear recurrent neural nets over sequence length. In *International Conference on Learning Representations*, 2018. URL <https://openreview.net/forum?id=HyUNwulC->.

Nakajima, K. and Fischer, I. *Reservoir computing*. Springer, 2021.

Orvieto, A., Smith, S. L., Gu, A., Fernando, A., Gulcehre, C., Pascanu, R., and De, S. Resurrecting recurrent neural networks for long sequences. In *International Conference on Machine Learning*, pp. 26670–26698. PMLR, 2023.

Pascanu, R., Mikolov, T., and Bengio, Y. On the difficulty of training recurrent neural networks. In Dasgupta, S. and McAllester, D. (eds.), *Proceedings of the 30th International Conference on Machine Learning*, volume 28 of *Proceedings of Machine Learning Research*, pp. 1310–1318, Atlanta, Georgia, USA, 17–19 Jun 2013. PMLR. URL <https://proceedings.mlr.press/v28/pascanu13.html>.

Pinna, M., Ceni, A., and Gallicchio, C. Residual reservoir memory networks. In *2025 International Joint Conference on Neural Networks (IJCNN)*, pp. 1–7. IEEE, 2025.

Rodan, A. and Tino, P. Minimum complexity echo state network. *IEEE Trans. Neural Netw.*, pp. 1–14, 01 2011.

Smith, J. T., Warrington, A., and Linderman, S. W. Simplified state space layers for sequence modeling. *arXiv preprint arXiv:2208.04933*, 2022.

Tay, Y., Dehghani, M., Bahri, D., and Metzler, D. Efficient transformers: A survey. *ACM Comput. Surv.*, 55(6), December 2022. ISSN 0360-0300. doi: 10.1145/3530811. URL <https://doi.org/10.1145/3530811>.

Tino, P. Dynamical systems as temporal feature spaces. *Journal of Machine Learning Research*, 21(44):1–42, 2020.

Vaswani, A., Shazeer, N., Parmar, N., Uszkoreit, J., Jones, L., Gomez, A. N., Kaiser, Ł., and Polosukhin, I. Attention is all you need. In *Advances in neural information processing systems*, pp. 5998–6008, 2017. URL <http://arxiv.org/abs/1706.03762>.

Verstraeten, D., Schrauwen, B., d’Haene, M., and Stroobandt, D. An experimental unification of reservoir computing methods. *Neural networks*, 20(3):391–403, 2007.

Verstraeten, D., Dambre, J., Dutoit, X., and Schrauwen, B. Memory versus non-linearity in reservoirs. In *The 2010 international joint conference on neural networks (IJCNN)*, pp. 1–8. IEEE, 2010.

Verzelli, P., Alippi, C., Livi, L., and Tino, P. Input representation in recurrent neural networks dynamics. *arXiv preprint arXiv:2003.10585*, 2020.

Yıldız, I. B., Jaeger, H., and Kiebel, S. J. Re-visiting the echo state property. *Neural networks*, 35:1–9, 2012.

Zhou, H., Zhang, S., Peng, J., Zhang, S., Li, J., Xiong, H., and Zhang, W. Informer: Beyond efficient transformer for long sequence time-series forecasting. In *Proceedings of the AAAI conference on artificial intelligence*, volume 35, pp. 11106–11115, 2021.

A. Table of contents for the Appendix

The Appendix is organized as follows:

- Appendix **B** provides a computational complexity analysis.
- Appendix **C** provides the paper's main proofs.
- Appendix **D** provides useful definitions about concepts used in our theoretical analysis.
- Appendix **E** provides details on the considered datasets.
- Appendix **F** discusses the experimental methodology.
- Appendix **G** presents additional experiments, covering hyperparameters' sensitivity and a comparison between the proposed approach and other reservoir computing approaches based on structured transforms.

B. Computational complexity

Here, we compare the time and space complexity of ParalESN, traditional ESNs, and other RC approaches based on structured transforms, including SCR (Rodan & Tino, 2011) and Structured RC (Dong et al., 2020). For simplicity, we consider the case of shallow, single-layer architectures and omit the computational cost of training the readout, as this cost is the same for all models. Table 5 provides an overview of the computational complexity analysis. Regarding time complexity, the diagonal transition matrix of ParalESN allows for a number of operations that scales linearly in the reservoir size N_h . Furthermore, the linear recurrence, which makes it possible to compute all time steps in parallel via associative scan, removes the linear dependency on the sequence length, reducing it to logarithmic. Regarding space complexity, ParalESN significantly reduces the memory footprint of its parameters compared to traditional ESNs by employing a diagonal transition matrix, storing only N_h diagonal elements rather than a full $N_h \times N_h$ matrix. This is crucial in enabling the construction of larger reservoirs.

ESN. We denote with $\{x_1, \dots, x_T\}$ an input sequence of length T , where each $x_i \in \mathbb{R}^{N_{\text{in}}}$. A standard nonlinear ESN with N_h hidden units updates its reservoir state according to Equation 1. Each time step requires two matrix-vector multiplications: one with the transition matrix ($N_h \times N_h$) and one with the input weight matrix ($N_h \times N_{\text{in}}$). Thus, the time complexity for processing the entire sequence is $\mathcal{O}(T(N_h^2 + N_h N_{\text{in}})) = \mathcal{O}(TN_h^2)$, where the equality assumes $N_{\text{in}} < N_h$, as is usual in ESNs. Regarding space complexity, ESNs store a full $N_h \times N_h$ transition matrix, a full $N_h \times N_{\text{in}}$ input weight matrix, and an N_h -dimensional bias vector. The space complexity for the model's parameters is $\mathcal{O}(N_h(N_h + N_{\text{in}}))$. The space complexity for the recurrence is $\mathcal{O}(TN_h)$, as we need to store T hidden states⁴.

SCR. The transition matrix employs a ring topology parameterization. The state update can be implemented in $\mathcal{O}(N_h)$ time, including the multiplication of the state by a scaling factor ρ . The time complexity is the same as a sequential ParalESN, $\mathcal{O}(TN_h N_{\text{in}})$. Regarding space complexity, SCR only stores a full $N_h \times N_{\text{in}}$ input weight matrix and an N_h -dimensional bias vector. The transformation applied by its transition matrix, arranged as a ring topology, simply shifts the vector elements and does not need to be stored. The space complexity for the model's parameters is $\mathcal{O}(N_h N_{\text{in}})$. The space complexity for the recurrence is the same as in traditional ESNs, $\mathcal{O}(TN_h)$.

Structured RC. The full transition matrix \mathbf{W}_h in (1) is replaced by a composition of Hadamard and diagonal matrices, reducing the time complexity by a log factor in the reservoir size and achieving $\mathcal{O}(TN_h \log N_h)$, assuming $N_{\text{in}} < \log N_h$. If the Hadamard matrix is stored explicitly, the space complexity for the model's parameters is the same as in traditional ESNs, $\mathcal{O}(N_h(N_h + N_{\text{in}}))$, though each element can be stored using a single bit rather than full floating-point precision since the matrix is binary. Alternatively, if the Hadamard transform is applied algorithmically via the fast Hadamard transform, no explicit storage is required, and only the diagonal matrices and input weights need to be stored, yielding a space complexity of $\mathcal{O}(N_h N_{\text{in}})$ for the model's parameters. The space complexity for the recurrence is the same as in traditional ESNs, $\mathcal{O}(TN_h)$.

ParalESN. In our approach, the reservoir update uses a diagonal transition matrix, which reduces the per-step computation to $\mathcal{O}(N_h N_{\text{in}})$. Hence, the sequential computation over a length- T sequence has total cost $\mathcal{O}(TN_h N_{\text{in}})$. Furthermore,

⁴ Assuming the case where we are interested in all time steps.

Table 5. Overview of time and space complexity.

MODEL	TIME COMPLEXITY SINGLE STEP	TIME COMPLEXITY WHOLE SEQUENCE	SPACE COMPLEXITY PARAMETERS	SPACE COMPLEXITY RECURRENCE
ESN	$\mathcal{O}(N_h^2)$	$\mathcal{O}(TN_h^2)$	$\mathcal{O}(N_h(N_h + N_{in}))$	$\mathcal{O}(TN_h)$
SCR	$\mathcal{O}(N_h N_{in})$	$\mathcal{O}(TN_h N_{in})$	$\mathcal{O}(N_h N_{in})$	$\mathcal{O}(TN_h)$
STRUCTURED RC	$\mathcal{O}(N_h \log N_h)$	$\mathcal{O}(TN_h \log N_h)$	$\mathcal{O}(N_h N_{in})$	$\mathcal{O}(TN_h)$
PARALESN	$\mathcal{O}(N_h N_{in})$	$\mathcal{O}(\log(T) N_h N_{in})$	$\mathcal{O}(N_h N_{in})$	$\mathcal{O}(TN_h)$

because state updates are linear, the computation can be parallelized along the temporal dimension. Using a parallel associative scan algorithm (Martin & Cundy, 2018), the dependence on T is reduced to a logarithmic factor⁵, yielding an overall complexity of $\mathcal{O}(\log(T) N_h N_{in})$. ParalESN stores the N_h elements of its diagonal transition matrix, a $N_h \times N_{in}$ input weight matrix, and an N_h -dimensional bias vector; thus, the space complexity for the model's parameters is $\mathcal{O}(N_h N_{in})$. The space complexity for the recurrence is the same as in traditional ESNs, $\mathcal{O}(TN_h)$.

Note that the associative scan could in principle be applied to any linear recurrence RC model, but practical limitations remain. Because the algorithm involves repeatedly squaring the transition matrix, it would in general require N_h^3 operations per scan step for full, unstructured matrices. Moreover, in the case of Structured RC, the matrix-matrix multiplication would create a full matrix, destroying the Hadamard structure.

C. Proofs

C.1. Proof of Theorem 4.1

We first prove the sufficient condition. Let \mathbf{h}_0 and \mathbf{h}'_0 be two vectors in \mathbb{C}^{N_h} , $\mathbf{x}_1, \dots, \mathbf{x}_N$ be a sequence of inputs, and $\rho(\bar{\Lambda}_h) < 1 - \epsilon$ be the spectral radius of $\bar{\Lambda}_h$. Because $\bar{\Lambda}_h$ is diagonal, it holds $\rho(\bar{\Lambda}_h) = \|\bar{\Lambda}_h\|_2$. Then,

$$\begin{aligned}
 \|\mathbf{h}_N - \mathbf{h}'_N\|_2 &= \|\bar{\Lambda}_h \mathbf{h}_{N-1} + \tau(\mathbf{W}_{in} \mathbf{x}_N + \mathbf{b}) - \bar{\Lambda}_h \mathbf{h}'_{N-1} - \tau(\mathbf{W}_{in} \mathbf{x}_N + \mathbf{b})\|_2 \\
 &= \|\bar{\Lambda}_h(\mathbf{h}_{N-1} - \mathbf{h}'_{N-1})\|_2 \\
 &\leq \|\bar{\Lambda}_h\|_2 \cdot \|(\mathbf{h}_{N-1} - \mathbf{h}'_{N-1})\|_2 \\
 &= \rho(\bar{\Lambda}_h) \cdot \|(\mathbf{h}_{N-1} - \mathbf{h}'_{N-1})\|_2 \\
 &\leq (1 - \epsilon) \cdot \|(\mathbf{h}_{N-1} - \mathbf{h}'_{N-1})\|_2 \\
 &\vdots \\
 &\leq (1 - \epsilon)^N \cdot \|\mathbf{h}_0 - \mathbf{h}'_0\|_2 \xrightarrow{N \rightarrow \infty} 0.
 \end{aligned}$$

This proves the sufficient condition. To prove the necessary condition, suppose that some diagonal entry $\bar{\lambda}_i$ of $\bar{\Lambda}_h$ satisfies $|\bar{\lambda}_i| > 1$. Then given two initial states $\mathbf{h}_0, \mathbf{h}'_0$ such that $(\mathbf{h}_0)_i \neq (\mathbf{h}'_0)_i$, unrolling the linear recursion we get the explicit formulas for \mathbf{h}_N and \mathbf{h}'_N :

$$\mathbf{h}_N = \bar{\Lambda}_h^N \mathbf{h}_0 + \sum_{j=1}^N \bar{\Lambda}_h^{N-j} \tau(\mathbf{W}_{in} \mathbf{x}_j + \mathbf{b}) \quad (11)$$

$$\mathbf{h}'_N = \bar{\Lambda}_h^N \mathbf{h}'_0 + \sum_{j=1}^N \bar{\Lambda}_h^{N-j} \tau(\mathbf{W}_{in} \mathbf{x}_j + \mathbf{b}) \quad (12)$$

Subtracting the two terms, we obtain

$$\mathbf{h}_N - \mathbf{h}'_N = \bar{\Lambda}_h^N (\mathbf{h}_0 - \mathbf{h}'_0). \quad (13)$$

Focusing on component i , we obtain that $(\mathbf{h}_N)_i - (\mathbf{h}'_N)_i = \bar{\lambda}_i^N ((\mathbf{h}_0)_i - (\mathbf{h}'_0)_i)$. Since $(\mathbf{h}'_0)_i \neq (\mathbf{h}_0)_i$ and $|\bar{\lambda}_i| > 1$, this term never reaches 0, growing exponentially in magnitude.

⁵Assuming $\Theta(T/\log T)$ parallel processors.

C.2. Proof of Proposition 4.2

Every square matrix is diagonalizable in the complex field, up to arbitrarily small perturbations in its entries, so we can write $\mathbf{W}_h = \mathbf{V}\Lambda_h\mathbf{V}^{-1}$, with $\mathbf{V} \in \mathbb{C}^{N_h \times N_h}$, and Λ_h a diagonal matrix, having on the diagonal the eigenvalues of \mathbf{W}_h . We can rewrite the recurrence in terms of \mathbf{V} and Λ as

$$\mathbf{h}_t = \mathbf{V}\Lambda_h\mathbf{V}^{-1}\mathbf{h}_{t-1} + \mathbf{W}_{\text{in}}\mathbf{x}_t. \quad (14)$$

Pre-multiplying each side of (14) by \mathbf{V}^{-1} , we get a complex diagonal ESN having the equations

$$\begin{cases} \tilde{\mathbf{h}}_t = \Lambda_h \tilde{\mathbf{h}}_{t-1} + \tilde{\mathbf{W}}_{\text{in}} \mathbf{x}_t \\ \mathbf{y}_t = \mathbf{W}_{\text{out}}(\sigma(\tilde{\mathbf{W}}_h \tilde{\mathbf{h}}_t)) \end{cases}$$

where $\tilde{\mathbf{h}}_t = \mathbf{V}^{-1}\mathbf{h}_t$, $\tilde{\mathbf{W}}_{\text{in}} = \mathbf{V}^{-1}\mathbf{W}_{\text{in}}$, and $\tilde{\mathbf{W}}_h = \mathbf{W}_h\mathbf{V}$. Therefore, for any possible linear ESN and for any sequence of inputs, there exists an equivalent complex diagonal ESN that, when given the same inputs, produces the same outputs.

D. Filters and Fading Memory Property

Here, we provide a broad overview of the definitions used to characterize the class of filters that ESNs and linear ESNs can universally approximate. Specifically, we introduce the concept of fading memory filters. We will mainly follow (Grigoryeva & Ortega, 2018a) and we point to it for further details.

Filters. Informally, a filter is a function that takes semi-infinite sequences and returns (semi)infinite sequences. More precisely, given $N_x \in \mathbb{N}$ and $N_y \in \mathbb{N}$, we define a filter \mathcal{U} as follows:

$$\mathcal{U} : (\mathbb{R}^{N_x})^{\mathbb{Z}_-} \rightarrow (\mathbb{R}^{N_x})^{\mathbb{Z}_-}, \quad (15)$$

where $(\mathbb{R}^N)^{\mathbb{Z}_-}$ is the set containing the semi-infinite sequences of vectors of dimension N , that are indexed by negative integer numbers (0 included)⁶, $\tilde{\mathbf{v}} = (\mathbf{v}_i)_{i \in \mathbb{Z}_-}$ with $\mathbf{v}_i \in \mathbb{R}^N$.

Two useful properties we would like for filters are *causality* and *time-invariance*. A filter \mathcal{U} is causal if its input at time t , $\mathbf{y}_t = \mathcal{U}(\tilde{\mathbf{x}})_t$ only depends on the inputs up until time t , i.e. $\tilde{\mathbf{x}}|_{(-\infty, t]}$. Causality of the target function is an intuitively useful property in tasks such as forecasting or autoregressive generation: without this property, seeing the past inputs could not be sufficient to determine univocally the present output. A filter is said to be time-invariant if, when given in input two shifted inputs, it outputs two sequences shifted by the same amount. Formally, for any positive integer $\tau > 0$, we can define the *time-shift operator* \mathcal{T}_τ as $\mathcal{T}_\tau(\tilde{\mathbf{x}})_t = \tilde{\mathbf{x}}|_{t-\tau}$. A filter is time-invariant if it commutes with the time-shift operator. This property is also useful, because it ensures that the filter definition does not depend explicitly on time t .

Infinite norm. The space $(\mathbb{R}^N)^{\mathbb{Z}}$ can be endowed with a norm, giving us a notion of distance. In particular, given a the usual euclidean norm for vectors $\|\cdot\|$, we define the *infinite norm* of a sequence as the supremum of the norm of any vector of the sequence.

$$\|\tilde{\mathbf{v}}\|_\infty = \sup_{i \in \mathbb{Z}} \|\mathbf{v}_i\|. \quad (16)$$

A *distance* between two sequences $\tilde{\mathbf{v}}$ and $\tilde{\mathbf{w}}$ can then be defined as the infinite norm of their difference:

$$d_\infty(\tilde{\mathbf{v}}, \tilde{\mathbf{w}}) = \|\tilde{\mathbf{v}} - \tilde{\mathbf{w}}\|_\infty. \quad (17)$$

Weighted norm: Intuitively, when measuring the difference between two sequences, often we would like to “count” more recent values more than ones distant in the past. Since infinite norm counts all values equally, this norm cannot achieve this important requirement. Therefore, we introduce a *weighting sequence* $w = (w)_i \in (0, 1]^{\mathbb{Z}_-}$, such that $\lim_{i \rightarrow -\infty} w_i = 0$, and define the *weighted norm* as:

$$\|\tilde{\mathbf{v}}\|_w = \|w \odot \tilde{\mathbf{v}}\|_\infty, \quad (18)$$

where \odot is the element-wise product.

⁶We could also define filters for infinite sequence, i.e. with inputs and outputs indexed by \mathbb{Z} . However, since in practice we are mainly interested in the “last” point of the sequences, it is common to restrict the definition to semi-infinite sequences.

Fading memory property: Finally, we can give a formal definition of fading memory property. The class of filters with fading memory property is the family of function that ESNs, and their linear counterparts, approximate arbitrarily well, thus making them universal. A fading memory filter is, simply put, a filter that is continuous when considering the distance induced by any weighted norm $\|\cdot\|_w$:

Definition D.1. A filter $\mathcal{U} : (\mathbb{R}^{N_x})^{\mathbb{Z}_-} \rightarrow (\mathbb{R}^{N_y})^{\mathbb{Z}_-}$ has the fading memory property if for any $\overleftarrow{\mathbf{x}}_1 \in (\mathbb{R}^{N_x})^{\mathbb{Z}_-}$ and $\epsilon > 0$, it exists $\delta = \delta(\epsilon) > 0$ such that if for any $\overleftarrow{\mathbf{x}}_2 \in (\mathbb{R}^{N_x})^{\mathbb{Z}_-}$ that satisfies

$$\|\overleftarrow{\mathbf{x}}_1 - \overleftarrow{\mathbf{x}}_2\|_w < \delta,$$

then

$$\|\mathcal{U}(\overleftarrow{\mathbf{x}}_1) - \mathcal{U}(\overleftarrow{\mathbf{x}}_2)\|_w < \epsilon. \quad (19)$$

ESNs have been proved universal in approximating arbitrarily well *time-invariant, causal filters with the fading memory property* (Grigoryeva & Ortega, 2018a) (Theorem 4.1).

E. Datasets

E.1. Memory-based

MemCap. The MemCap task involves outputting a delayed version of the input k time steps in the past. The memory capacity score, used to assess performance on the MemCap task, is computed by summing the squared correlation coefficients between the k -th time step delayed version of the input and the output for each delay value $k = 1, \dots, 200$. We generate an input sequence uniform in $[-0.8, 0.8]$ with length $T = 7000$. The first 5000 time steps are used for training, the next 1000 for validation, and the final 1000 for testing. Both training and inference employ a 100 time step washout to warm up the reservoir.

ctXOR. Consider a one-dimensional input time series $\mathbf{x}(t)$ uniformly distributed in $(-0.8, 0.8)$ and assume $\mathbf{r}(t-d) = \mathbf{x}(t-d-1)\mathbf{x}(t-d)$. The task is to output the time series $\mathbf{y}(t) = \mathbf{r}(t-d)^2 \text{sign}(\mathbf{r}(t-d))$, where d is the delay and p determines the strength of the non-linearity. We consider delay $d = 5$ (ctXOR5) and delay $d = 10$ (ctXOR10).

SinMem. Given a one-dimensional input time series $\mathbf{x}(t)$ uniformly distributed in $(-0.8, 0.8)$, the task is to output the time series $\mathbf{y}(t) = \sin(\pi\mathbf{x}(t-d))$. For SinMem, we consider delays $d = 10$ (SinMem10) and $d = 20$ (SinMem20).

E.2. Forecasting

Lorenz96. The Lorenz96 task is to predict the next state of the time series $\mathbf{x}(t)$, expressed as the following 5-dimensional chaotic system:

$$\mathbf{x}(t) = \frac{\partial}{\partial t} f_i(t) = f_{i-1}(t)(f_{i+1}(t) - f_{i-2}(t)) - f_i(t) + 8, \quad (20)$$

for $i = 1, \dots, 5$. In our experiments, we focus on predicting the 25-th (Lz25) and 50-th (Lz50) future state of the time series. Thus, the task involves predicting $\mathbf{y}(t) = \mathbf{x}(t+25)$ and $\mathbf{y}(t) = \mathbf{x}(t+50)$, respectively. We generate a time series of length $T = 1200$. The first 400 time steps are used for training, the next 400 for validation, and the final 400 for testing.

Mackey-Glass. The Mackey-Glass 17 (MG) task is to predict the next state of the following time series:

$$\mathbf{x}(t) = \frac{\partial}{\partial t} f(t) = \frac{0.2f(t-17)}{1 + f(t-17)^{10} - 0.1f(t)}. \quad (21)$$

In our experiments, we focus on predicting the 1-st and 84-th future state of the time series. Thus, the task involves predicting $\mathbf{y}(t) = \mathbf{x}(t+1)$ (MG) and $\mathbf{y}(t) = \mathbf{x}(t+84)$ (MG84), respectively. We generate a time series of length $T = 10000$, with the first 5000 time steps used for training, the next 2500 for validation, and the final 2500 for testing.

NARMA. Given a one-dimensional input time series $\mathbf{x}(t)$ uniformly distributed in $[0, 0.5]$, the NARMA task is to predict the next state of the following time series:

$$\mathbf{y}(t) = 0.3\mathbf{y}(t-1) + 0.01\mathbf{y}(t-1) \sum_{i=1}^d \mathbf{y}(t-i) + 1.5\mathbf{x}(t-d)\mathbf{x}(t-1) + 0.1. \quad (22)$$

We will consider the NARMA10 (N10) and NARMA30 (N30), with look-ahead delay of $d = 10$ and $d = 30$, respectively. We generate a time series of length $T = 10000$, with the first 5000 time steps used for training, the next 2500 for validation, and the final 2500 for testing.

Real-world datasets. The ETTh1, ETTh2, ETTm1, and ETTm2 (Zhou et al., 2021) represent real-world and challenging forecasting tasks. In Table 6 an overview of their characteristics. We focus on the multivariate case and predict all provided features. We use a delay of 192 time steps. We normalize each feature in the training set independently to zero mean and unit variance. The normalization coefficients computed on the training data are then applied to normalize the validation and test data. Since we observe order-of-magnitude outliers in the training set, we clip the normalized training data to the interval $(-10, 10)$ across all datasets. The validation and test data remain unmodified.

Table 6. Overview of the real-world forecasting datasets. Training, validation, and test sizes are measured in the number of time steps.

DATASET	TRAIN	VALIDATION	TEST	# FEATURES
ETTH1/2	8640	2880	2880	7
ETTM1/2	34560	11520	11520	7

E.3. Classification

In Table 7 an overview of the considered classification datasets. The validation set is obtained via a 90 – 10 stratified split for sMNIST and psMNIST, and via a 70 – 30 stratified split for other tasks. No data augmentation is applied.

Table 7. Overview of time series and 1-D pixel-level classification tasks.

DATASET	TRAIN	TEST	LENGTH	# FEATURES	# CLASSES
BLINK	500	450	510	4	2
FAULTDETECTIONA	10912	2728	5120	1	3
FORDA	3601	1320	500	1	2
FORDB	3636	810	500	1	2
sMNIST/psMNIST	60000	10000	784	1	10
STARLIGHTCURVES	1000	8236	1024	1	3

F. Experimental setting

F.1. Computational resources

Experiments are run on a system with 4×18 -core Intel Xeon Gold 6140M CPUs @ 2.30 GHz (144 threads total) and $4 \times$ NVIDIA Tesla V100-PCIE-16GB GPUs. To track computational efficiency metrics, such as training time, energy consumption, and emissions, we use CodeCarbon (Courty et al., 2024).

F.2. Model selection

Model selection is carried out via Bayesian search, exploring configurations up to a maximum runtime of 24hrs. The best configuration is chosen based on the performance achieved on the validation set.

For RC models, Table 8 provides an overview of the values explored. Common hyperparameters explored for both ESN and ParalESN include the bias scaling ω_b , the leaky rate τ , and the number of layers L . For traditional RC we explore the spectral radius ρ , used to rescale the recurrent weight matrix, and the input scaling ω_{in} , used to scale the input weight matrix. For ParalESN, we explore the minimum and maximum magnitude of the diagonal entries ρ_{min} , ρ_{max} , and the minimum and maximum phase (i.e., the angle with the positive x-axis) θ_{min} , θ_{max} , used to sample the diagonal transition matrix

Table 8. Hyperparameters for RC models.

HYPERPARAMETERS	VALUES
concat	[False, True]
L	[1, 2, 3, 4, 5]
ω_b and inter- ω_b	{0, 0.01, 0.1, 1, 10}
τ and inter- τ	{0.1, 0.5, 0.9, 1}
(ESN)	
ω_{in} and inter- ω_{in}	{0.01, 0.1, 1, 10}
ρ and inter- ρ	{0.1, 0.5, 0.9}
(ParalESN)	
<i>(Reservoir)</i>	
ρ_{max} and inter- ρ_{max}	{0.1, 0.5, 0.9}
ρ_{min} and inter- ρ_{min}	{0, 0.1, 0.5, 0.9}
θ_{max} and inter- θ_{max}	{ $\frac{1}{2}\pi$, π , 2π }
θ_{min} and inter- θ_{min}	{0, $\frac{1}{2}\pi$, π , 2π }
<i>(Mixer)</i>	
ω_{mix} and inter- ω_{mix}	{0.01, 0.1, 1, 10}
ω_{mixb} and inter- ω_{mixb}	{0, 0.01, 0.1, 1, 10}
k and inter- k	{3, 5, 7, 9}

and easily control its eigenvalues. Additionally, we explore ω_{mix} and ω_{mixb} for scaling the kernel and the bias vector of the mixing layer, and k for determining the kernel size. For the deep configurations, we explore the number of (untrained) reservoir layers L and we explore an additional set of hyperparameters for layers beyond the first one, to promote diverse dynamics between the first layer and deeper ones. Additionally, we consider hyperparameter `concat` \in [False, True], which determines whether the readout is fed the states of the last layer or the concatenation of the states across all layers. To ensure a consistent number of trainable parameters when states are concatenated, the hidden size (i.e., the total number of reservoir units) is evenly split across layers. If an even split is not possible, the remaining neurons are allocated to the first layer. When the readout is implemented as a ridge regressor, we explore regularization strength values in $\{0, 0.01, 0.1, 1, 10, 100\}$. When the readout is implemented as an MLP, we simply train it with the Adam optimizer with a learning rate of $5e-4$; the rest are the default PyTorch values. See Table 8 for an overview of the values explored. The readout is either implemented as a ridge regressor trained via Singular Value Decomposition (SVD) solver for memory-based, forecasting, and time series classification tasks, or as a 2-layer Multi-layer Perceptron (MLP) for benchmarks pertaining to the MNIST dataset. Prior to the readout, we always standardize the reservoir’s outputs by removing the mean and scaling to unit variance.

For fully-trainable models, we employ the Adam optimizer and sweep through the learning rate with a log uniform distribution over the interval $[0.0001, 0.01]$, and the weight decay exploring values in $\{0, 1e-7, 1e-6, 1e-5, 1e-4, 1e-3, 1e-2, 1e-1\}$. For LRU, we also sweep through ρ_{\min} with uniform distribution over the interval $[0, 1]$, ρ_{\max} with uniform distribution over the interval $[0.8, 1]$, and θ_{\max} with uniform distribution over the interval $[0.001, 3.14]$. The LSTM employs a hidden size of 192, the Transformer employs an input size of 96 and a feedforward size of 128 for 3 encoder layers, LRU employs 3 layers with hidden size of 82, Mamba employs 6 layers with model dimension 64, state expansion factor 16, and local convolutional width 4. We train fully-trainable models and the MLP of ParalESN, for at most 100 epochs and with an early-stopping mechanism, to avoid inflating the computational efficiency metrics. For classification, the readout or classification head of each model are fed only the state at the last time step.

G. Additional experiments

G.1. Hyperparameters’ sensitivity

In Fig. 6, we explore ParalESN’s hyperparameter sensitivity on the NARMA10 benchmark. For simplicity, we consider a shallow, single-layer ParalESN. For the reservoir layer, the spectral radius, phase, and leaky rate appear to be critical hyperparameters, with significant error increases when these are not tuned properly. In contrast, minor effects are observed for the bias scaling. For the mixing layer, the most important hyperparameter is the input scaling of the kernel, while its bias scaling and kernel size have relatively smaller effects on performance.

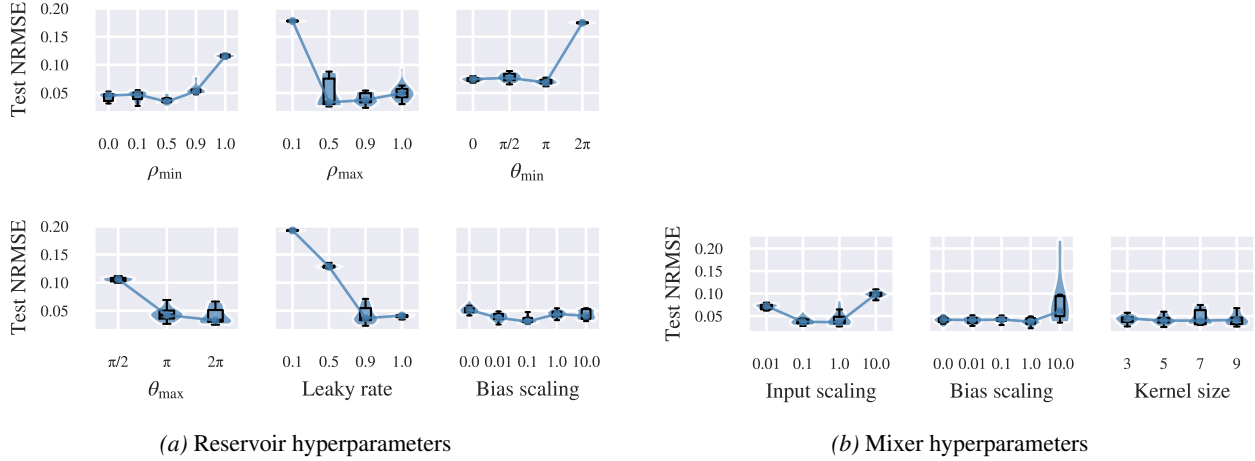


Figure 6. Analysis of ParalESN’s hyperparameter sensitivity for (a) the reservoir and (b) the mixer, on the NARMA10 tasks.

Table 9. Comparison of structured reservoir computing approaches on time series forecasting, assuming 128 recurrent neurons for each model. A traditional ESN is included as a baseline. Top-two results are underlined, **best result** is in bold.

FORECASTING	$\cdot 10^{-2}$ Lz25 (↓)	$\cdot 10^{-2}$ Lz50 (↓)	$\cdot 10^{-4}$ MG (↓)	$\cdot 10^{-2}$ MG84 (↓)	$\cdot 10^{-2}$ N10 (↓)	$\cdot 10^{-2}$ N30 (↓)
ESN	10.0 ± 0.3	30.8 ± 0.6	3.0 ± 0.0	6.5 ± 0.4	2.7 ± 0.4	10.3 ± 0.1
SCR	22.1 ± 0.4	35.6 ± 0.8	18.7 ± 4.2	32.2 ± 3.1	11.1 ± 0.2	16.1 ± 0.9
Structured RC	10.4 ± 0.2	30.9 ± 0.5	12.6 ± 0.1	28.5 ± 1.6	18.7 ± 0.1	20.9 ± 0.1
ParalESN	10.4 ± 0.5	30.2 ± 0.5	2.8 ± 0.2	7.4 ± 0.4	3.7 ± 0.8	10.2 ± 0.1

G.2. Comparison with structured reservoir computing

Here, we compare ParalESN with other reservoir computing approaches based on structured transforms on time series forecasting benchmarks. We consider Simple Cycle Reservoir (SCR) (Rodan & Tino, 2011) and Structured Reservoir Computing (Structured RC) (Dong et al., 2020)⁷. For both SRC and Structured RC, model selection employs the same methodology described in Section F. Note that in SCR, there is no need to tune the spectral radius since the transition matrix employs a fixed ring topology. In Structured RC, rather than tuning the spectral radius of the transition matrix, we tune the reservoir scaling for values in [0.01, 0.1, 1, 10]. Although traditional ESNs are not based on structured transforms, we include their results as a baseline.

Table 9 presents results. For simplicity, we consider a shallow configuration of one layer for all models. ParalESN is consistently one of the top-performing models along with ESN, while other approaches based on structured transforms consistently underperform across all datasets. In particular, compared to SCR and Structured RC, ParalESN achieves lower test error on MG, MG84, and N10 by an entire order of magnitude and half the error on N30.

⁷Code from github.com/rubenohana/Reservoir-computing-kernels.